Structure, Vol. 12, 703–715, April, 2004, ©2004 Elsevier Science Ltd. All rights reserved. DOI 10.1016/j.str.2004.03.001

X-Ray Structure Determination of Three Mutants of the Bacterial Photosynthetic Reaction Centers from *Rb. sphaeroides*: Altered Proton Transfer Pathways

Qiang Xu, Herbert L. Axelrod, Edward C. Abresch, Mark L. Paddock, Melvin Y. Okamura, and George Feher*
Department of Physics
University of California, San Diego
9500 Gilman Drive
La Jolla, California 92093

Summary

In the photosynthetic reaction center (RC) from *Rhodobacter sphaeroides*, the reduction of a bound quinone molecule Q_B is coupled with proton uptake. When Asp-L213 is replaced by Asn, proton transfer is inhibited. Proton transfer was restored by two second-site revertant mutations, Arg-M233→Cys and Arg-H177→His. Kinetic effects of Cd^{2+} on proton transfer showed that the entry point in revertant RCs to be the same as in the native RC. The structures of the parental and two revertant RCs were determined at resolutions of 2.10, 1.80, and 2.75 Å. From the structures, we were able to delineate alternate proton transfer pathways in the revertants. The main changes occur near Glu-H173, which allow it to substitute for the missing Asp-L213. The electrostatic changes near Glu-H173 cause it to be a good proton donor and acceptor, and the structural changes create a cavity which accommodates water molecules that connect Glu-H173 to other proton transfer components.

Introduction

Proton transfer is a fundamental process in biological energy transduction. It involves membrane and water soluble proteins in such diverse systems as photosynthesis and respiration (Silverman, 2000; Lanyi and Luecke, 2001; Lancaster, 2002; Neutze et al., 2002; Decoursey, 2003; Mills and Ferguson-Miller, 2003). Pathways for proton transfer from the exterior to the catalytic site consist of ionizable amino acid side chains and bound water molecules. Site-directed mutagenesis combined with high-resolution structure determinations of several of these proteins have helped to identify specific amino acid residues that are important for proton transfer, thereby allowing proton pathways to be delineated. The goal of these investigations is to understand how specific structural features of the pathways promote fast and efficient proton transfer. The bacterial photosynthetic reaction center (RC) is a good model system for studying the details of the proton transfer process. The best characterized of these RCs is that from *Rhodobacter* (*Rb.*) *sphaeroides*.

The bacterial RC is a membrane bound pigment-protein complex that converts light energy into chemical energy (reviewed by Feher et al., 1989; Gunner, 1991; Blankenship et al., 1995; Hoff and Deisenhofer, 1997). The absorption of a photon by the primary electron donor, a bacteriochlorophyll dimer (D), triggers a series of electron transfer steps between the cofactors imbedded inside the protein. The electron is transferred from D via a bacteriopheophytin to the primary quinone, Q_A, and subsequently to the secondary quinone, Q_B. The reaction is coupled with proton uptake to the residue Glu-L212 near Q_B (Paddock et al., 1989; Takahashi and Wraight, 1992; Hienerwadel et al., 1995; Nabedryk et al., 2000). The reaction proceeds with an observed rate constant $k_{AB}^{(1)}$ as shown in Equation 1.

$$H + (Q_A^{-\bullet}\, Q_B)Glu^- \xrightarrow{k_{AB}^{(1)}} (Q_A Q_B^{-\bullet})GluH, \qquad (1)$$

where Glu^- is the ionized form of Glu-L212. The electron transfer and proton uptake are strongly coupled, i.e., the electron transfer cannot proceed without the protonation of Glu-L212. Consequently, measuring electron transfer by optical spectroscopy provides a means to monitor proton uptake. After the oxidized primary donor, D^+, is rereduced by the secondary electron donor cytochrome c_2, a second photon is absorbed and an electron is again transferred to Q_A. The second electron transfer from $Q_A^{-\bullet}$ to the semiquinone $Q_B^{-\bullet}$ is also intimately coupled to proton uptake, which involves Asp-L213 and Ser-L223, and occurs with a rate constant $k_{AB}^{(2)}$ as described by Equation 2a (Graige et al., 1996),

$$H^+ + (Q_A^{-\bullet}\, Q_B^{-\bullet})GluH \xrightarrow{k_{AB}^{(2)}} (Q_A\, Q_B H^-)GluH \qquad (2a)$$

Subsequent proton transfer from Glu-L212 to reduced Q_B results in the formation of quinol,

$$(Q_A Q_B H^-)GluH \rightarrow (Q_A Q_B H_2)Glu^- \qquad (2b)$$

The overall reaction for the double reduction of Q_B is

$$Q_B + 2e^- + 2H^+ \rightarrow Q_B H_2 \qquad (3)$$

The end product, dihydroquinone, leaves the quinone binding site and is replaced by a neutral quinone from the free quinone pool in the cytoplasmic membrane.

The proton transfers coupled to the electron transfer steps (Equations 1 and 2) in the RC from *Rb. sphaeroides* and other purple bacteria have been extensively investigated using both optical kinetics (reviewed in Okamura and Feher, 1995; Okamura et al., 2000) and computational methods (Beroza et al., 1995; Lancaster et al., 1996; Rabenstein et al., 1998; Sham et al., 1999; Alexov and Gunner, 1999; Alexov et al., 2000). Residues that are essential for the proton transfer have been identified by site-directed mutagenesis. The X-ray crystal structure of the RC (e.g., Stowell et al., 1997) shows that several of these residues are in close proximity to $Q_B^{-\bullet}$ (Figure 1). For example, Ser-L223 is within hydrogen bonding distance of one carbonyl oxygen of $Q_B^{-\bullet}$, and two acid residues, Asp-L213 and Glu-L212, are ~3 Å away from the methoxy groups of $Q_B^{-\bullet}$ (Figure 1). Site-directed mutagenesis results show that the replacement

*Correspondence: gfeher@ucsd.edu

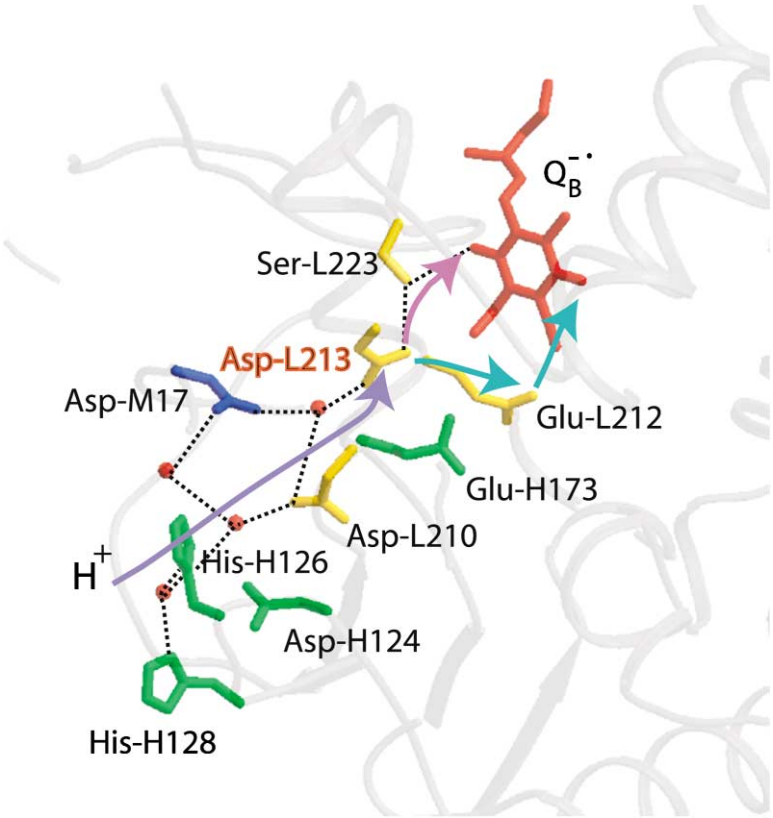

Figure 1. The Dominant Proton Transfer Pathways to Reduced Q_B in the Native Reaction Center of *Rb. Sphaeroides*, PDB Accession Code: 1AIG

Amino acid side chains from the L subunit are shown in yellow, M in blue, and H in green. Part of the protein backbone is shown in gray. The actual proton pathways are indicated by the dotted lines, while the arrows give the general direction of the proton transfer. The purple arrow indicates the path for both the first and second proton uptake from solution to Asp-L213. The pathways for the two protons diverge after Asp-L213. The magenta arrow shows the path for the first proton transfer (Equation 2a), while the turquoise arrows show the path for the second proton transfer (Equations 1 and 2b). Water molecules that constitute the proton pathways are shown in red. The Glu-H173 side chain has a relatively large B factor of ~70 Å^2 comparing to the average for the whole protein of ~55 Å^2, indicating disorder. The illustration is made with program BOBSCRIPT (Esnouf, 1999) and RASTER3D (Merritt and Bacon, 1997).

of Asp-L213 with Asn [*DN(L213)*] inhibits the proton uptake (Equation 2a) as does the replacement of Ser-L223 (Paddock et al., 1990, 1994; Takahashi and Wraight, 1990, 1992; Leibl et al., 1993), whereas replacement of Glu-L212 with Gln inhibits the internal protonation shown in Equation 2b and the subsequent proton uptake shown in Equation 1 (Paddock et al., 1989; Takahashi and Wraight, 1992). Thus, two functionally different proton transfer pathways leading to the two carbonyl oxygens of Q_B exist in the RC.

The molecular details of the proton transfer pathways were deduced from X-ray crystal structures. The catalytic Q_B site is buried inside the RC. From the X-ray crystal structure one can deduce several different possible proton transfer pathways connecting Q_B to the cytoplasmic surface each with a unique proton entry point (Beroza et al., 1992; Ermler et al., 1994; Baciou and Michel, 1995; Stowell et al., 1997; Abresch et al., 1998). The subsequent finding that the binding of a single divalent metal ion, such as Zn^{2+} (Utschig et al., 1998) or Cd^{2+}, to the RC surface inhibited both proton uptake steps (Equations 1 and 2a) showed that there was a unique proton entry that was shared by both proton pathways (Paddock et al., 1999; Ädelroth et al., 2000). The location of the metal binding site was determined by X-ray crystallography to be at the cytoplasmic surface of the H subunit, with the metal ion coordinated to His-H126, His-H128, and Asp-H124 (Axelrod et al., 2000). This region was confirmed to be the proton entry point by showing that the decrease in the rates of proton uptake resulting from the removal of the imidazole groups (His→Ala mutation) was the same as that in the native RCs with a bound Cd^{2+} (Ädelroth et al., 2001).

The dominant proton uptake pathways in the native RC are shown in Figure 1 (Axelrod et al., 2000; Paddock et al., 2000). The first proton enters through His-H126 or His-H128, passes via Asp-L210 and/or Asp-M17 and bound waters to proceed to Asp-L213, then to Ser-L223, which facilitates delivery of the first proton to $Q_B^{-\bullet}$ (Equation 2a). The second proton enters the protein at the same location and travels along the same pathway as the first proton up to Asp-L213 where it branches off to proceed to Glu-L212, which donates the second proton to Q_BH^- (Equation 2b) following the second electron transfer reaction (Equation 2a).

These proton transfer pathways are inhibited when Asp-L213 is replaced with Asn [*DN(L213)*]. The most drastic consequence of this replacement is a ~10^6 fold decrease (to 0.1 s^{-1}) in the proton uptake associated with Equation 2a (Paddock et al., 1998), which changes the rate-limiting step of Equation 2a from electron transfer to proton transfer. This reduced rate results in a nonviable RC, i.e., the mutant cannot grow photosynthetically. However, the RC has been shown to be quite robust and a large number of distinct phenotypic second-site revertants have been isolated in *Rb. sphaeroides* and *Rb. capsulatus* (Hanson et al., 1992, 1993; Rongey et al., 1993; Paddock et al., 1998; Miksovska et al., 1998; Alexov et al., 2000). In *Rb. sphaeroides,* three of these revertant RCs of the lethal *DN(L213)* mutation have been kinetically characterized. They are as follows: *DN(L213)/ND(M44)*, which has the Asn-M44→Asp re-

vertant mutation; *DN(L213)/RC(M233)*, which has the Arg-M233→Cys revertant mutation; and *DN(L213)/RH(H177)*, which has the Arg-H177→His revertant mutation (Paddock et al., 1998).

The *DN(L213)/ND(M44)* RC is kinetically the most similar to the native RC (Paddock et al., 1998). The M44 side chain is in close proximity of L213 and Ser-L223 (within 4 Å of both residues in the native structure), which suggests that the carboxylic acid of the M44 side chain substitutes for Asp-L213 as part of the proton transfer pathways. This provides an explanation for the presence of an Asp at either L213 or M44 (*Rb. sphaeroides* numbering) in all photosynthetic bacteria. However, a more complicated explanation is required to understand the partial restoration of proton uptake in revertants in which the revertant mutation site is either farther from L213 and $Q_B^{-\bullet}$ or does not introduce a new carboxylic acid side chain. For example, in the revertant [*DN(L213)/RC(M233)*], the site of the revertant mutation at M233 is located ~13 Å from the initial Asn-L213 lesion and ~17 Å from $Q_B^{-\bullet}$. Measurements on isolated revertant reaction centers showed that the proton uptake rate increased at least four orders of magnitude above that of the lethal *DN(L213)* mutant. Two explanations have been proposed for the enhancement of the proton transfer rate involving unspecified structural changes that either (1) propagate over relatively long distances to locations near L213 and $Q_B^{-\bullet}$ (Sebban et al. 1995; Paddock et al., 1998) and/or (2) activate an alternate proton pathway in the revertant (Hanson et al., 1992 , 1993). To distinguish between these two possibilities and to provide a more detailed molecular model for possible structural changes that restore function, high-resolution structures of the parental mutant and the revertants are needed.

The goal of this study was to determine the nature of the structural changes induced by the revertant mutations and to understand how these changes lead to a restoration of fast proton transfer. To achieve this goal, we crystallized the *DN(L213)* mutant RC and two phenotypic revertants *DN(L213)/RC(M233)* and *DN(L213)/RH(H177)* and determined their X-ray crystal structures to resolutions of 2.10, 1.80, and 2.75 Å, respectively. An inspection of these structures led us to postulate altered proton pathways. Preliminary accounts of this work have been presented (M.L. Paddock et al., 1999, Biophys. J., abstract 76, A141; Q. Xu et al., 2003, Biophys. J., abstract 84, 273a).

Results

Structure of the *DN(L213)* Mutant

To identify structural changes due to mutations at the revertant site, we first determined the structure of the parental *DN(L213)* mutant RC. The structure has been refined to an R factor of 21.1% (R_{free} = 22.8%) at a resolution of 2.10 Å (Table 1).

The structure of the polypeptide backbone of the *DN(L213)* RC is essentially the same as that of the native RC (rms deviation of 0.4 Å) (PDB accession code: 1AIJ) (Stowell et al., 1997). The position of Q_B in the *DN(L213)* structure (Figure 2) is the same as that observed in the charge separated state ($D^+Q_B^{-\bullet}$) in the native RC (PDB accession code: 1AIG), which is displaced by ~5 Å toward Ser-L223 and His-L190 compared to that of the native RC in the charge neutral state. This is not surprising as $Q_B^{-\bullet}$ is likely to be the prevalent state in the *DN(L213)* mutant due to its enhanced stability over the neutral Q_B (by ~90 meV at pH 8.0 [Labahn et al., 1994]). An additional contribution to the enhanced fraction of $Q_B^{-\bullet}$ may be due to the room light used in manipulating and freezing the crystal.

The side chains of the residues of the *DN(L213)* mutant are similar to that of the light-adapted RC (1AIG), except some changes near Glu-H173 (Figure 2). The electron density of this residue in several native structures has been reported to be weak, indicating disorder (Stowell et al., 1997; Pokkuluri et al., 2002). In contrast, in the *DN(L213)* mutant RC, the electron density for the side chain of Glu-H173 is found to be stronger but bifurcated. We modeled the side chain of Glu-H173 as two alternate conformations each with a 50% occupancy. In addition, each conformation has an associated water molecule (see Figure 2). The two conformations form different interactions with nearby residues. In one conformation (cyan in Figure 2), the side chain of Glu-H173 is within hydrogen bonding distance of the side chain of Asn-L213 while the side chain in the other conformation (yellow in Figure 2) is within salt bridging distance of the guanidinium side chain of Arg-H177. The carboxyl group in both conformations is also within hydrogen bonding distance to the hydroxyl group of Thr-L226. The implication of the two conformations of Glu-H173 is discussed in a later section.

Structure of the *DN(L213)/RC(M233)* Revertant *Dark-Adapted State*

The *DN(L213)/RC(M233)* has been crystallized in two crystal forms, $P3_121$ (trigonal) and $P4_32_12$ (tetragonal), and the dark-adapted structures were refined to 1.80 and 2.40 Å, respectively (see Table 1). The higher resolution of 1.80 Å allowed a better fit of residue side chains and the identification of a greater number of bound water molecules, which are important for the delineation of the proton pathway. The structural changes near the revertant mutation site and near Glu-H173, described below, are the same in the trigonal and tetragonal forms. In both forms, the secondary quinone is in the distal position, the same as in the native dark-adapted structure. This is consistent with its lower redox potential compared to that of the *DN(L213)* RC (Paddock et al., 1998). The only significant differences between the structures in the two crystal forms are at the molecular contact regions.

Changes Near the Revertant Site. The most significant structural differences between the *DN(L213)/RC(M233)* revertant and the parental *DN(L213)* mutant RC occur near the revertant site M233. The electron density at M233 confirms the substitution of the smaller Cys for the larger Arg. The amino acid replacement breaks the salt bridge formed with Glu-H230. However, a new salt bridge is formed between Glu-H230 and Arg-H177, which moves into the cavity created by the mutation (Figure 3A). Side chains of two nearby acidic residues

Table 1. X-Ray Data Collection and Refinement Statistics

Mutant	*DN(L213)*	*DN(L213)/RC(M233)*	*DN(L213)/RC(M233)*	*DN(L213)/RC(M233)* ($D^+ Q_B^{-\bullet}$)	*DN(L213)/RH(H177)*
Crystal data					
Space group	$P3_121$	$P3_121$	$P4_32_12$	$P4_32_12$	$P3_121$
a = b (Å)	139.1	139.5	139.6	137.7	138.2
c (Å)	184.6	185.2	274.7	277.1	184.4
Maximum resolution (Å)	2.10	1.80	2.40	2.60	2.75
Total observations (unique)	710,388 (118,004)	765,939 (188,278)	517,218 (117,357)	343,061 (78,285)	364,591 (53,191)
Mean $I/\sigma(I)$[a] (highest resolution shell)	6.5 (2.0)	5.4 (2.0)	7.2 (1.9)	4.4 (2.3)	7.4 (2.0)
R_{sym}[b] (highest resolution shell) (%)	9.8(37.8)	9.8 (34.1)	9.1 (36.7)	8.6 (38.5)	8.2 (36.7)
Completeness[c] (highest resolution shell) (%)	98.2 (96.9)	98.6 (99.5)	97.4 (89.3)	95.3 (82.5)	99.6 (99.4)
Refinement					
Resolution range	40–2.10	40–1.80	40–2.40	40–2.60	40–2.75
R factor[d] (%)	21.1	22.1	21.5	22.8	21.8
R_{free}[e] (%)	22.8	23.2	24.8	26.5	23.7
Deviation from ideal bond length (Å)	0.011	0.011	0.016	0.012	0.011
Deviation from average bond angle (°)	1.4	1.4	1.6	1.5	1.8
Rms coordinate error[f] (Å)	0.3	0.3	0.3	0.4	0.3
Average B factor (Å^2)	37	28	43	57	57
Ramachandran plot					
Residues in most favored regions (%)	92.2	92.3	90.2	89.3	91.9
Residues in additional allowed regions (%)	7.5	7.4	9.5	10.5	7.7
Residues in generously allowed regions (%)	0.3	0.3	0.3	0.3	0.4
Residues in disallowed regions	0	0	0	0	0

[a] $I/\sigma(I)$ is the ratio of the average of the diffraction intensities to the average background intensity.
[b] $R_{sym} = \Sigma_{hkl,j}(|I_{hkl} - \langle I_{hkl}\rangle|)/\Sigma_{hkl,j} I_{hkl}$, where $\langle I_{hkl}\rangle$ is the average intensity for a set of j symmetry-related reflections and $\langle I_{hkl}\rangle$ is the value of the intensity for a single reflection within a set of symmetry-related reflections.
[c] Completeness is the ratio of the number of reflections measured to the total number of possible reflections.
[d] R factor = $\Sigma_{hkl}(||Fo| - |Fc||)/\Sigma_{hkl}|Fo|$, where Fo is the observed structure factor amplitude and Fc is the calculated structure factor amplitude.
[e] $R_{free} = \Sigma_{hkl,T}(||Fo| - |F_c||)/\Sigma_{hkl,T}|F_o|$, where a test set, T (5% of the data), is omitted from the refinement.
[f] Rms error in coordinates based on the method of Luzzati (Luzzati, 1952).

Glu-H122 and Glu-M236 also shift by 4–6 Å, with Glu-M236 moving closer to and Glu-H122 moving further from Arg-H177. The movement of Arg-H177 breaks its salt bridge with Glu-H173 by increasing the distance from the N atoms of the granidinium group of Arg-H177 to the oxygen atoms of the carboxyl group of Glu-H173 to 10 Å.

Other basic and acidic residues nearby, e.g., Arg-H117, Lys-H130, Glu-H230 and Glu-M232, also respond to the loss of the electrostatic interaction with Arg at M233 (data not shown), although their side chain displacements are relatively small (0.5–0.8 Å). In addition, there are some small rearrangements of noncharged groups, e.g., Met-H175 rotates around the CG-SD bond by ~120°.

Changes that Propagate Toward L213. The large structural changes that propagate to the region near the parental mutation at L213 and the Q_B catalytic site occur at Glu-H173 and Thr-L226. In this revertant, Glu-H173 can be modeled in a single conformation at a position between the two alternate conformations in the *DN(L213)* mutant (Figure 4). In addition, Thr-L226 rotates ~120° around the CA-CB bond, with the hydroxyl group now pointing away from Glu-H173, breaking its hydrogen bond with Glu-H173.

The movements of Glu-H173 and Thr-L226 create a cavity in the pocket surrounded by Asn-M44, Asn-L213, Glu-L212, Thr-L226, and Glu-H173. Within this cavity there are well-defined electron densities corresponding to two water molecules, W155 and W193 (Figure 4).

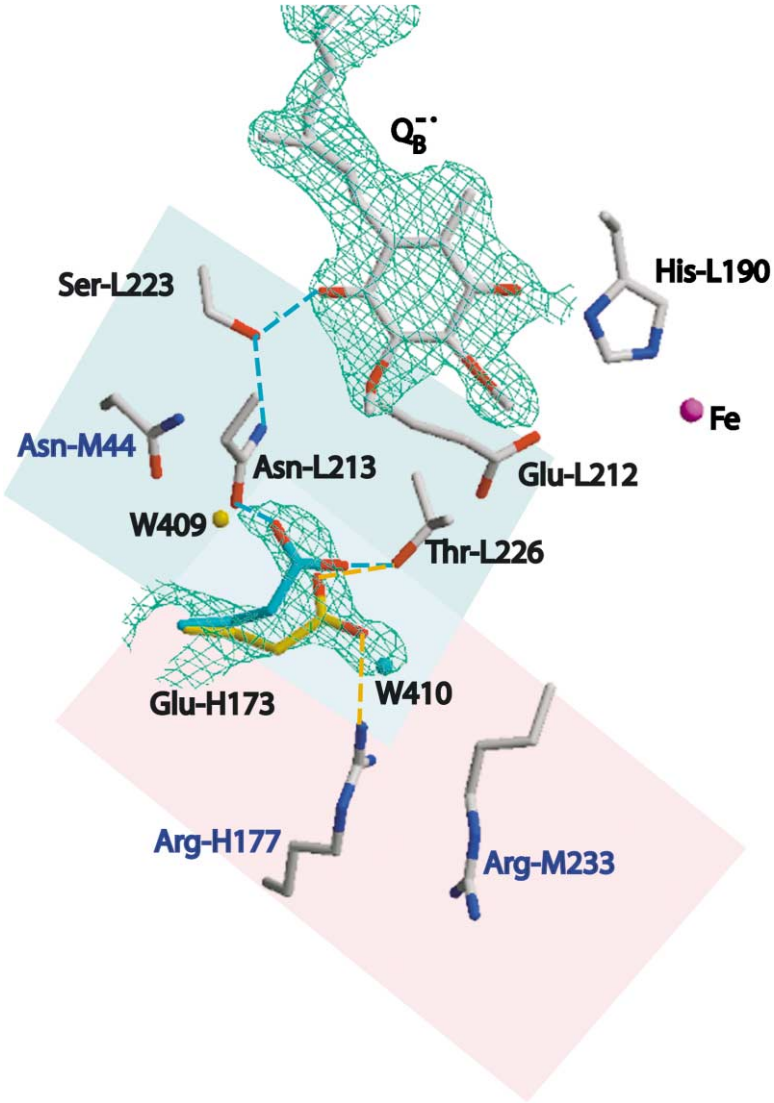

Figure 2. Structure Near the Secondary Quinone Q_B Binding Pocket in the *DN(L213)* Mutant

The three revertant mutation sites, M44, H177, and M233 are labeled in blue. The quinone is in the proximal position similar to that in the native, light-adapted RCs. The Glu-H173 side chain has two conformations (cyan and yellow) each with one associated water molecule colored correspondingly. The dashed lines indicate the potential hydrogen bonding network from Glu-H173 to the semiquinone in one conformation and the salt bridge with Arg-H177 in the other conformation. 2Fo-Fc electron density contoured at 1σ is superimposed on $Q_B^{-\bullet}$ and Glu-H173. The pink region contains the two revertant mutations that were investigated (see Figure 3), while the cyan region contains the parental *DN(L213)* mutation (see Figure 4).

Water W155 is 2.7 Å from Glu-H173 and 4.0 Å from Glu-L212 (see dotted lines in Figure 4). This water molecule is not observed in the native structures. Water W193 is 2.7 Å from Glu-H173 and 4.6 Å away from the side chain oxygen atom of Ser-L223, which is the first proton donor to the semiquinone (see dotted lines in Figure 4). It is also within hydrogen bonding distance of Asn-L213 (3.0 Å) and Asn-M44 (2.7 Å) (see dashed lines in Figure 4). This water molecule is at the same position as water W409 in the *DN(L213)* structure associated with one conformation of Glu-H173 (Figure 2). A water molecule at this position is also observed in a recently reported native RC structures (Katona et al., 2003).

Light-Adapted State

The tetragonal crystal of *DN(L213)/RC(M233)* was also frozen under illumination to trap the $D^+Q_B^{-\bullet}$ charge separated state. (Although the trigonal crystal of *DN(L213)/RC(M233)* diffracts to a higher resolution than the tetragonal form, the larger thickness of the crystal compared to the tetragonal form prevented the penetration of the light required to form the charge separated state throughout the crystal). The structure of the light-adapted state was refined to a resolution of 2.60 Å. No significant differences in the polypeptide structure are observed compared to the dark-adapted structure. Thus, the structural changes of the revertant discussed in the previous section are also observed in the light-adapted structure. The two water molecules near Glu-H173 discussed above are not resolved in the light structure, although they can be inferred from the voids in the structure. The electron density at the Q_B site indicates more disorder in the position of Q_B, compared to the dark-adapted state. This is presumably due to a distribution of the Q_B density, consistent with fractional occupancies of Q_B in both the proximal and distal position. However, the electron density is not of sufficient quality to reliably model its position. EPR spectra on the biradical $Q_A^{-\bullet}Q_B^{-\bullet}$, which are sensitive to the relative orientation of $Q_A^{-\bullet}$ and $Q_B^{-\bullet}$ (Calvo et al., 2000), show no difference between the revertant *DN(L213)/RC(M233)* and the

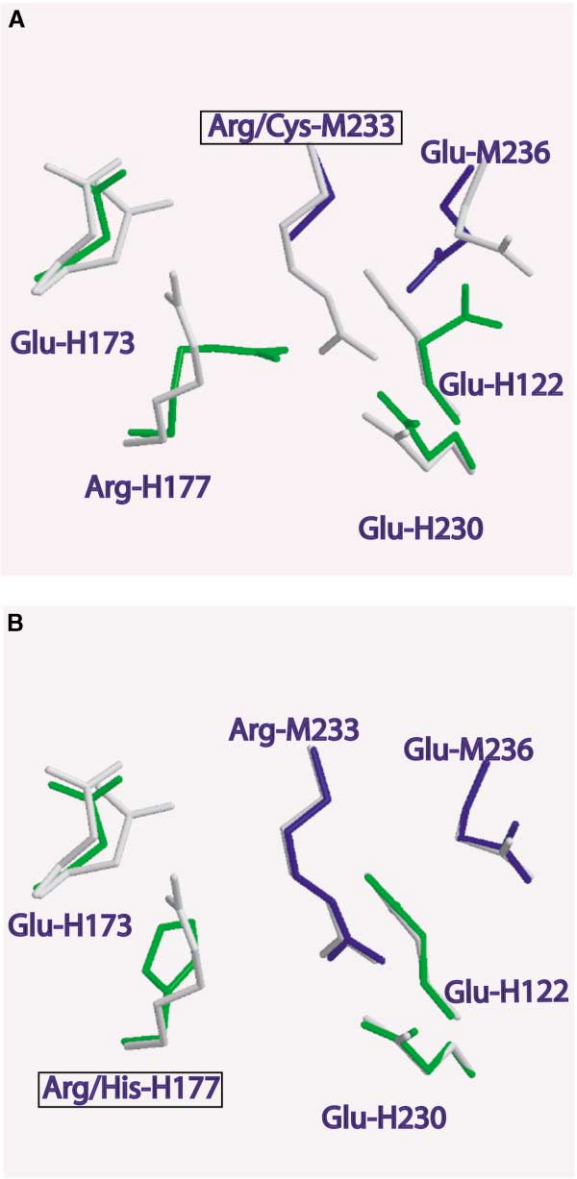

Figure 3. The Structures Near the Revertant Site in the *DN(L213)/RC(M233)* and in the *DN(L213)/RH(H177)* Revertant

The revertant sites are indicated by framed labels. For comparison, the *DN(L213)* structure (gray) is superimposed on the structures of the revertants. Both conformations of the Glu-H173 in the *DN(L213)* structure are shown. Color code for residues same as in Figure 1.

native RC (M.L.P., R. Calvo, E.C.A., M.Y.O., and G.F., unpublished data). We, therefore, conclude that $Q_B^{-\bullet}$ occupies the proximal site in the revertant.

Structure of the *DN(L213)/RH(H177)* Revertant

The structure of the *DN(L213)/RH(H177)* revertant in the trigonal form has been refined to an R factor of 21.5% (R_{free} = 23.6%) at a resolution of 2.75 Å (Table 1).

Changes Near the *Revertant* Site

The electron density at the revertant site is consistent with the replacement of Arg by His at H177 and the addition of two water molecules near H177. In contrast to the other revertant structure, no rearrangements of Arg-M233, Glu-M236, and Glu-H122 are observed compared to the *DN(L213)* mutant (Figure 3B).

Changes that Propagate toward L213

All major structural changes are in the vicinity of Glu-H173. The conformational changes of Glu-H173 (Figure 3B) and Thr-L226 (data not shown) are the same as in the other revertant (Figure 4). The salt bridge between Glu-H173 and Arg-H177 in the parental *DN(L213)* mutant has been broken. The two water molecules near Glu-H173 discussed in the *DN(L213)/RC(M233)* revertant (Figure 4) are not resolved but could be modeled into the vacant cavities.

Binding of Cd^{2+} to Mutant RCs

It has been shown that the binding of Zn^{2+} (Utschig et al., 1998) or Cd^{2+} to the RC surface decreased the proton uptake rate by binding near the proton entry point (Paddock et al., 1999). To assess if the proton entry point was altered, the mutant RCs were tested for metal sensitivity.

The rate of transfer of the second electron to Q_B ($k_{AB}^{(2)}$) after the second saturating laser flash at 450 nm was measured at different Cd^{2+} concentrations in all three mutant RCs. Representative traces of the optical absorbance changes after the second laser flash of the mutant [*DN(L213)/RH(H177)*] are shown in Figure 5. The data were fitted with the sum of two exponentials: one (slow) corresponding to the reaction of RCs with a bound Cd^{2+} and one (fast) corresponding to RCs without a bound Cd^{2+}. The rates of $k_{AB}^{(2)}$ at high (saturating) concentrations of Cd^{2+} together with $k_{AB}^{(2)}$ in the absence of Cd^{2+} are summarized in Table 2.

From a plot of the fraction of RCs exhibiting slow kinetics as a function of Cd^{2+} concentration, a binding curve for Cd^{2+} was constructed. A fit to a single binding site isotherm yielded the dissociation constants of K_D = 4 ± 1 μM for *DN(L213)/RH(H177)* and 6 ± 1 μM for *DN(L213)/RC(M233)*. The value of K_D for the native RC is 0.3 μM. In addition, the pH dependence of K_D can be modeled as was done for the native RC (Gerencser and Maroti, 2001; Paddock et al., 2003) to yield a pK_a of ~7 for the metal ligand of the histidine.

Discussion

In this work we determined the structural changes in two phenotypic revertants of proton uptake inhibited RCs from *Rb. sphaeroides*. The rate of proton uptake coupled to the electron transfer reactions (Equation 2a) is reduced ~10^6-fold in RCs in which Asp-L213 is replaced by Asn (Table 2) (Paddock et al., 1998). This results in a photosynthetically incompetent RC. Several second-site revertant mutations were found to increase proton transfer function to a sufficient level to restore photosynthetic competence (Rongey et al., 1993; Paddock et al., 1998). In this work we focused on two revertants that had second-site mutations located far from the original L213 mutation and that did not reintroduce a carboxylic acid as a possible substitute for the removed Asp-L213. Although structural changes had been invoked as the reason for the restored function (Hanson et al., 1992, 1993; Paddock et al., 1998), no details about

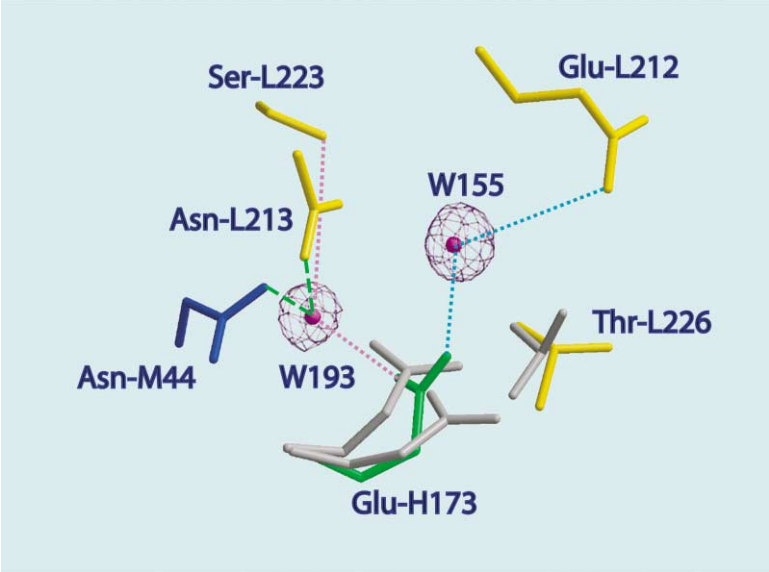

Figure 4. The Structure Near Glu-H173 in the Dark-Adapted *DN(L213)/RC(M233)* Revertant

Glu-H173 (both conformations) and Thr-L226 residues of the *DN(L213)* structure (gray) are superimposed for comparison on the structure of the revertant. Color code of residues same as in Figure 1. Two resolved water molecules, W193 and W155, bridge Glu-H173 to Ser-L223 and Glu-L212 as shown by dotted lines (magenta and turquoise respectively), and form part of the proton path. W193 is also hydrogen bonded to Asn-M44 and Asn-L213 (green line). 2Fo-Fc electron densities for the two water molecules are contoured at 1.5σ.

the nature of the changes had been previously reported. In this work we determined the high-resolution structures of the parental lethal mutation Asp-L213→Asn [*DN(L213)*] and of the revertants Asp-L213→Asn/Arg-M233→Cys [*DN(L213)/RC(M233)*] and Asp-L213→Asn/Arg-H177→His [*DN(L213)/RH(H177)*]. From the detailed structure of the mutants, we were able to postulate alternate proton transfer pathways. These are compared with the predominant pathway in the native RC.

Structural Changes Induced by the Mutations

In this section we review the structural changes in the mutant RC crystal structures. We begin with a discussion of the changes observed in the *DN(L213)* mutant which has the detrimental Asp-L213→Asn mutation. The backbone conformation and, for the most part, the side chain conformations of the mutant are essentially the same as in the native RC. In the DN(L213) structure reported here, the most pronounced change occurs in the position of Glu-H173 which, in contrast to the native RC structure, exists in two conformations with approximately equal occupancy. Glu-H173 is located between the parental L213 mutation site and the revertant sites at M233 and H177 (see Figure 2). In one conformation (cyan in Figure 2), Glu-H173 is hydrogen bonded to Asn-L213, which creates a potential H-bonded chain connecting the protonated Glu-H173 via Asn-L213 and Ser-L223 with $Q_B^{-\bullet}$. This requires that in this conformation Glu-H173 be protonated. In the other conformation (yellow in Figure 2), Glu-H173 is near Arg-H177 (~4.0 Å), forming a potential salt bridge only if Glu-H173 is ionized, i.e., unprotonated, in this position. Such an interaction, using Coulomb's law and assuming a dielectric constant of 20 (Antosiewicz et al., 1996), yield an energy of 200 meV, favoring the ionized state. Thus, in one conformation Glu-H173 is protonated, whereas in the other it is ionized (unprotonated).

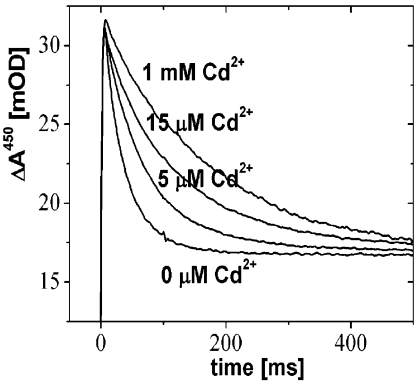

Figure 5. The Effect of Adding Cd^{2+} on the Second Electron Transfer Rate, $k_{AB}^{(2)}$, after the Second Laser Flash in the Photosynthetic Revertant *DN(L213)/RH(H177)*

Conditions: 1 μM RC, 10 mM HEPES, pH 7.5, 0.04% maltoside. $CdCl_2$ added to the concentrations indicated.

Next we examine the revertant RC structures, which showed more significant changes. The largest of them were found in the *DN(L213)/RC(M233)* RC near the site of the revertant mutation at M233. The revertant mutation results in the replacement of Arg with Cys which removes the positive charge and most of the side chain length. As a result, several nearby charged groups reorient. The most striking are (1) the movement of Arg-H177 which now places its guanidinium group in the region vacated by the revertant mutation and (2) the rearrangements of several Glu side chains to form new salt bridges that replace the ones lost upon changing Arg-M233 to Cys. Such a cascade of rearrangements due to the loss of a charged group, termed "electrostatic dominos" (Sebban et al., 1995), provide a means to propagate changes to the Q_B and L213 sites. Such rearrangements are not observed in the other revertant structure in which Arg-H177 was changed to a His. Since the kinetic behaviors of the two revertant RCs are essentially the same (Paddock et al., 1998), there must be other structural changes common to both revertants that account for their similarly restored activities.

Table 2. The Observed Rate Constant $k_{AB}^{(2)}$ in the Absence and Presence of Saturating Concentration of Cd^{2+} and the Proton Transfer Rate Constant $k_H^{(1)}$, pH 7.5

System	$k_{AB}^{(2)}$ (0) (s^{-1})	$k_{AB}^{(2)}$ (Cd) (s^{-1})	($k_{AB}^{(2)}$ (0))/ ($k_{AB}^{(2)}$ (Cd))	$k_H^{(1)}$ (s^{-1})
NATIVE	1200	120	10	$\sim 10^5$
DN(L213)	0.25	0.20	1	0.25
DN(L213)/RC(M233)	80	15	5	$>10^3$
DN(L213)/RH(H177)	40	10	4	$>10^3$

See Equation 2a for observed rate constant $k_{AB}^{(2)}$.

Similar changes were observed in both revertant RCs at and near Glu-H173. The main change is a unique conformation of Glu-H173 which differs from either of the two alternate conformations in the *DN(L213)* mutant. In this conformation, the salt bridge between Glu-H173 and H177 has been disrupted as well as the hydrogen bond with Thr-L226 (Figure 3 and 4). These changes enlarge the cavity surrounding Glu-H173, in which two water molecules are resolved in the higher resolution *DN(L213)/RC(M233)* RC structure. Water molecule W193 (Figure 4) provides part of a bridge between Glu-H173 and Ser-L223, which is a transient proton donor coupled with the second electron transfer (Equation 2a). Water molecule W155 (Figure 4) provides part of a bridge between Glu-H173 and Glu-L212, which is a proton donor coupled with the first electron transfer (Equation 1). Although these water molecules are not resolved in the lower resolution *DN(L213)/RH(H177)* structure, we infer their presence from the spaces (voids) that are present in the structure. We propose, therefore, that the conformational change of Glu-H173 and the incorporation of these water molecules are the functionally important changes.

Entry Point of Proton Uptake in the Revertants

As in the native RC, several potential proton transfer pathways connecting the Q_B site to the surface are possible with each pathway having a unique entry point on the surface. The entry point for the dominant pathway in the revertants was localized to the surface region near His-H126 and His-H128 by the inhibitory effect of a bound Cd^{2+} in a manner analogous to the native RC (Paddock et al., 1999; Axelrod et al., 2000) . The binding of Cd^{2+} resulted in a $\sim$5-fold decrease in $k_{AB}^{(2)}$ (Table 2), which is, within a factor of two, the same as in the native RC (Paddock et al., 1999). The binding curve indicates that the inhibition is due to binding of a single Cd^{2+} ion, as found for the native RC. The pH dependence of the binding affinity is consistent with an interaction between Cd^{2+} and His. We, therefore, conclude that the proton entry point is the same in the revertant RCs as in the native, i.e., near His-H126 and His-H128 (Axelrod et al., 2000). This conclusion is also consistent with the fact that the structure of the side chains (His-H126, His-H128, and Asp-H124) to which Cd^{2+} binds is unaffected in the revertant RCs.

Functional Consequences of the Structural Changes: Potential Proton Transfer Pathways

The main motivation to determine the structure of the mutant RCs was to provide the molecular basis for understanding the functional consequences of the mutations, in particular, the nonviable phenotype of the *DN(L213)* RC and the viable phenotype of the revertants *DN(L213)/RC(M233)* and *DN(L213)/RH(H177)* RCs. We start with a discussion of the single *DN(L213)* mutation in which proton transfer is inhibited. The structure along the proton transfer pathway is essentially the same as in the native RC. Thus, the inhibition is not due to structural changes but is a direct consequence of the lack of proton donating ability of the Asn as had previously been proposed (Takahashi and Wraight, 1990; Paddock et al., 1994).

Next we address the functional consequences of the structural changes observed in the revertant RCs. The basic question is how the protons bypass the Asn-L213 block in the revertant RCs. Since the two revertant structures are essentially identical in the region near Glu-H173 and Asn-L213, we focus on the higher resolution structure of the *DN(L213)/RC(M233)* RC. The revertant mutation results in structural changes that rearrange the region near Glu-H173 which allows it to substitute for the missing carboxylic acid at L213. Among these changes is rearrangement of the charged residue Arg-H177 (Figure 3A), which modifies the electrostatic environment to provide an appropriate pK_a of Glu-H173 to be a good proton donor and acceptor. In addition, water molecules W193 and W155 provide connectivity between Glu-H173 and the proton acceptors Ser-L223 and Glu-L212, respectively (Figure 6). Although the connection from Glu-H173 to Ser-L223 involves a gap of $\sim$4.6 Å, it is possible that there is an unresolved additional water molecule in this region to provide connectivity or that fluctuations of the protein transiently reduce the gap, creating an H-bonded proton path.

Another requirement is that Glu-H173 be connected to the surface region near His-H126 and His-H128. In analogy to the native RC, this connection is provided by Asp-L210 and/or Asp-M17 and several water molecules as shown in Figure 6. It should be noted that a second possible route involving a more contiguous water chain composed of seven water molecules is possible (data not shown).

The structural changes near Glu-H173 are common to both revertant RCs, in contrast to the structural changes induced at the revertant sites which are different. Note that although neither revertant mutation directly results in the incorporation of a carboxylic acid, the altered pathways involve a carboxylic acid (Glu-H173) that functionally serves as a substitute for the missing Asp at L213.

In the above discussion, we showed the important

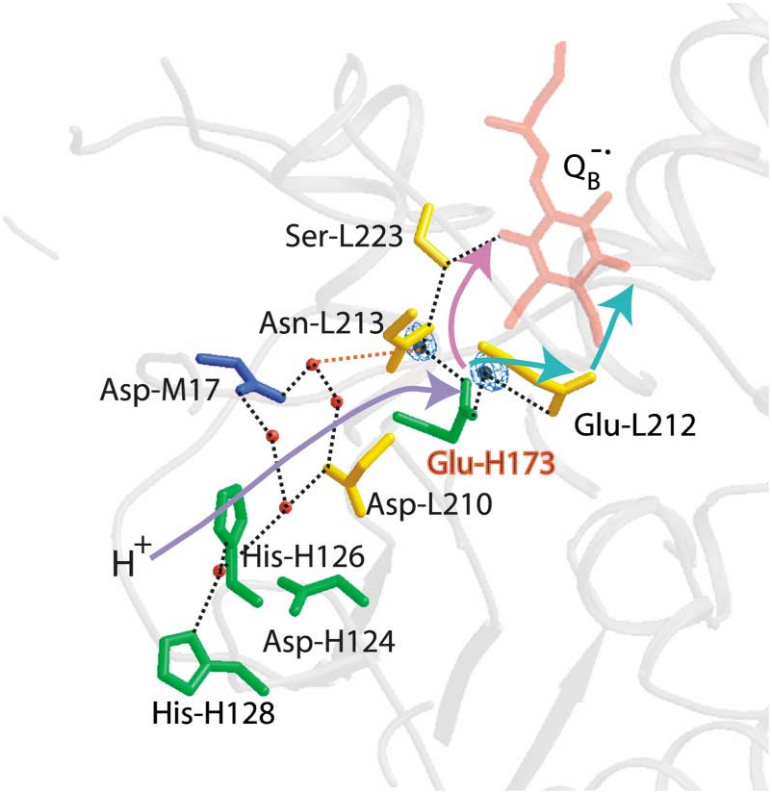

Figure 6. The Proton Pathways in the Revertant *DN(L213)/RC(M233)*

Color scheme for the side chains and arrows is the same as in Figure 1. Two water molecules near Glu-H173 are shown in black with their 2Fo-Fc electron densities contoured at 1.5σ. In addition to the two new water molecules, some of the other water molecules shown in red are not the same as in Figure 1, changing the detailed pathways shown by dotted lines. The dotted red line represents the largest gap of 4.6 Å between resolved water molecules. The pathways for the two protons now pass through Glu-H173 instead of Asp-L213 in the native structure (Figure 1).

role that Glu-H173 plays in the revertants. In contrast, it has been shown by site-directed mutagenesis (Takahashi and Wraight, 1996) that in the native RC, Glu-H173 is not a component of the proton pathway but may indirectly facilitate proton transfer by providing electrostatic stabilization to an internal proton on residues or waters of the proton transfer pathways.

Why Is Glu-H173 Not Effective in the *DN(L213)* Mutant?

In the structure of the *DN(L213)* RC, in which proton transfer is inhibited, Glu-H173 can assume two conformations. Since the two conformations are nearly equally occupied, we conclude that proton transfer does not occur with Glu-H173 in either conformation. Let us discuss each conformation separately. In the cyan conformation shown in Figure 2, Glu-H173 is part of a well-ordered hydrogen bonding chain connecting Glu-H173 to one oxygen of $Q_B^{-\bullet}$ (Figure 2). However, this chain is not effective in proton transport because the amide residue Asn in the chain cannot easily deprotonate, i.e., it cannot easily donate or accept a proton. In this conformation, Glu-H173 is not connected via a proton path to the proton acceptors Ser-L223 and Glu-L212. Thus, we conclude that the cyan conformer is not active in proton transfer.

In the second, yellow conformation shown in Figure 2, the water molecule W409 could provide connectivity between Glu-H173 and $Q_B^{-\bullet}$ as is found in the revertant RCs. However, it is difficult to protonate Glu-H173 at this position due to the strong interaction of the ionized form of Glu-H173 with the nearby Arg-H177. As discussed in the previous section, this interaction energy is estimated to be ~200 meV which results in lowering the pK_a of Glu-H173 by ~3 pH units. This interaction creates an electrostatic barrier for protonation of Glu-H173, which reduces its effectiveness as a protonatable residue. In many different revertant mutations (Hanson et al., 1993; Hanson and Schiffer, 1998), a net decrease in positive charge (Maroti et al., 1994) reduces this electrostatic barrier. We conclude, therefore, that the yellow conformer is also not active in proton transfer because of the electrostatic barrier that prevents the protonation of Glu-H173.

Thus, to have an effective proton transfer path, two conditions need to be fulfilled. An appropriate electrostatic environment is required to facilitate internal protonation, and proton connectivity is needed throughout the transfer chain. Both of these conditions are met in the revertants but not in the *DN(L213)* mutant.

Robustness of the Photosynthetic Reaction Center

There are many similarities between the native and revertant proton transfer pathways. They share the involvement of the surface region, in particular His-H126 and His-H128 and the intermediate carboxylic acids Asp-L210 and/or Asp-M17 connected via bridging water molecules (Figures 1 and 6). Each of these pairs provides a redundancy as either of the residue of each pair is sufficient for efficient proton transfer (Ädelroth et al., 2001; Paddock et al., 2001).

The restoration of proton transfer through the creation of an altered proton transfer pathway by a single amino

Table 3. Crystallization Conditions and Cryoprotectant Composition

	Tetragonal	Trigonal	
	DN(L213)/RC(M233) Dark and Light Adapted	*DN(L213)/RC(M233)*	*DN(L213), DN(L213)/RH(H177)*
Droplet 20–40 μl	7.7 mg/ml RC, 0.25 mg/ml Cytochrome c_2, 5% (w/v) PEG4000, 10 mM Tris-HCl, (pH 8.5), 0.1 mM EDTA, 0.06% LDAO, 3.9% (w/v) heptanetriol, 35 mM KCl.	10.1 mg/ml RC, 0.65 M potassium phosphate (pH 8.5), 0.09 mM NaCl, 0.1% LDAO, 2% (w/v) heptanetriol, 3% dioxane	10.1 mg/ml RC, 1.0 M potassium phosphate (pH 8.5), 0.09 mM NaCl, 0.1% LDAO, 2% (w/v) heptanetriol, 3% dioxane, 3% hexanetriol
Reservoir 1 ml	22% (w/v) PEG4000, 0.45 M NaCl, 10 mM Tris-Hcl (pH 8.5), 0.1 mM EDTA	1.4 M potassium phosphate (pH 8.5)	2.0 M potassium phosphate (pH 8.5)
Cryoprotectant	None	0.65 M potassium phosphate (pH 8.5), 0.09 mM NaCl, 0.1% LDAO, 2% (w/v) heptanetriol, 3% dioxane, 35% sucrose	1.3 M potassium phosphate (pH 8.5), 0.12 mM NaCl, 0.13% LDAO, 2.6% (w/v) heptanetriol, 3.9% dioxane, 3.9% hexanetriol, 35% glycerol

acid change is another aspect of the robust nature of the proton transfer pathways in the bacterial RC. There is a strict requirement for a single side chain at the residues near the Q_B catalytic site, such as Asp-L213. The structures of the revertants revealed that even the removal of this key residue can be overcome by structural rearrangements and a changed electrostatic environment resulting from a single amino acid change that allow a nearby Glu-H173 to substitute for the missing Asp at L213. The ability of the bacteria to create an alternate proton transfer pathway endows it with a flexibility to overcome detrimental mutations.

Concluding Remarks

The crystal structures provide explanations on a molecular level of the differences in proton transfer observed in the mutant *DN(L213)* and the *DN(L213)/RC(M233)* and *DN(L213)/RH(H177)* revertant RCs. The key differences involve the environment near Glu-H173 which allow it to substitute for the missing Asp at L213 in the revertant RCs but not in the parental *DN(L213)* RC. There are two factors that contribute to the efficiency of Glu-H173 as a proton transfer component. The first factor is the electrostatic environment of Glu-H173 which "tunes" its proton affinity so that it can effectively accept and donate a proton to other components of the proton transfer pathway. The second factor involves the structural changes that result in the creation of a cavity that can accommodate water molecules providing connectivity of Glu-H173 with other proton transfer pathway components.

Experimental Procedures

Protein Purification and Characterization

Construction of the Asp-L213→Asn [*DN(L213)*] revertant has been reported previously (Paddock et al., 1994), as has the isolation and characterization of the two photosynthetic revertant strains, Asp-L213→Asn/Arg-M233→Cys [*DN(L213)/RC(M233)*] and Asp-L213→Asn/Arg H177→His [*DN(L213)/RH(H177)*] (Paddock et al., 1998). RCs were isolated from semiaerobically grown cultures of the mutants using the detergent lauryldimethylamine-N-oxide (LDAO; Fluka) as described by Paddock et al. (Paddock et al., 1988). The purity of the sample was monitored by the optical ratio, A_{280nm}/A_{802nm}, which was <1.25 in all preparations.

Crystallization

Crystals of two previously reported crystal forms, tetragonal (space group $P4_32_12$) (Allen, 1994) and trigonal (space group $P3_121$) (Buchanan et al., 1993; Fritzsch et al., 2002), were obtained by vapor diffusion at 19°C in either 20 or 40 μl sitting drops with 1 ml reservoirs in Cryschem-type plates (Charles Supper Co., Natick, MA). The crystallization conditions are summarized in Table 3. Trigonal crystals were used for structure determinations of the *DN(L213)* and DN(L213)/RH(H177) mutants. The structure of the other revertant, *DN(L213)/RC(M233)*, was determined in both the tetragonal and trigonal crystal forms. Tetragonal crystals of this mutant were used for the structure determinations of RCs in the charge-separated state, $D^+ Q_B^{-\bullet}$.

Kinetics Measurement

Absorption changes in response to a laser flash were recorded on a modified Cary 14 spectrometer (Varian) as descried by Kleinfeld et al. (Kleinfeld et al., 1984). Actinic illumination was provided by a Nd-YAG laser (Opotek, Carlsbad, CA). The rate of second electron transfer from Q_A to Q_B ($k_{AB}^{(2)}$) was determined by monitoring the decay of the semiquinone absorption at 450 nm following a second laser flash in the presence of 20 μM horse heart cytochrome c as an external electron donor. To test the effect of metal ion binding on the kinetic rate, $CdCl_2$ was added to the RC sample at increasing concentrations.

X-Ray Data Collection

X-ray diffraction data were collected at a wavelength of 0.95 Å on crystals cooled to ~100 K at the Stanford Synchrontron Radiation Laboratory (SSRL) (Beamlines 9-1 and 9-2). To trap the light-adapted, charge-separated state, crystals were mounted on nylon loops, illuminated, and plunged into liquid nitrogen as described by Stowell et al. (Stowell et al., 1997) before placement onto a goniostat cooled to ~100 K during data collection. Data from a tetragonal crystal of the *DN(L213)/RC(M233)* mutant RC in the dark-adapted state was also collected. Trigonal crystals were similarly mounted on nylon loops but soaked in cryoprotectant solutions containing either sucrose or glycerol before being cooled with liquid nitrogen. The compositions of the cryoprotectants are summarized in Table 3. For the crystals treated with glycerol as a cryoprotectant, we confirmed that two to four cycles of reversible flash cooling improves the resolution by ~0.5 Å (Fritzsch et al., 2002). The diffraction data were integrated with the MOSFLM (Leslie, 1992) software packages and scaled with CCP4 SCALA (CCP4, 1994) program. Unit cell parameter and data processing statistics are shown in Table 1.

X-Ray Structure Determination

The 2.20 Å coordinates of the native RC in the dark-adapted state (PDB accession code 1AIJ) were used as a starting model for the refinement of the tetragonal crystal form of the *DN(L213)/RC(M233)* mutant in the dark-adapted state. The structure resulting from the refinement was in turn used as the starting model for the refinement in the light-adapted state of this mutant. For the three mutant structures in the trigonal form, the starting model was the 2.10 Å structure from McAuley et al. (McAuley et al., 1999) (PDB accession code 1QOV) with the Q_A site rebuilt according to the native dark structure (1AIJ).

Water, detergent molecules, and the coordinates of Q_B were omitted from the starting model prior to refinement. In the later stages of refinement, bound water molecules were added into Fo-Fc difference electron density peaks that are $>3\sigma$ above the background level of the map and within 4 Å of potential hydrogen bond donors and acceptors. Q_B and detergent molecules were also added at this stage. Rigid body, positional, simulated annealing, and isotropic temperature factor refinement were carried out with the CNS package (Brunger et al., 1998). Between each round of refinement, 2Fo-Fc and Fo-Fc electron density maps were calculated using the CNS package. The maps were inspected and the models were manually revised using the computer graphics program XtalView (McRee, 1999). The refinement statistics are listed in Table 1.

Acknowledgments

We thank C. Chang, R. Isaacson, and A. Yeh for technical assistance. This work has been supported by the National Institutes of Health (NIH Grants GM-13191 and GM 41637). Portions of this research were carried out at the Stanford Synchrotron Radiation Laboratory (SSRL), a national user facility operated by Stanford University on behalf of the U.S. Department of Energy, Office of Basic Energy Sciences. The SSRL Structural Molecular Biology Program is supported by the Department of Energy, Office of Biological and Environmental Research, and by the National Institutes of Health, National Center for Research Resources, Biomedical Technology Program, and the National Institute of General Medical Sciences.

Received: December 15, 2003
Revised: February 3, 2004
Accepted: February 4, 2004
Published: April 6, 2004

References

Abresch, E.C., Paddock, M.L., Stowell, M.H.B., McPhillips, T.M., Axelrod, H.L., Soltis, S.M., Rees, D.C., Okamura, M.Y., and Feher, G. (1998). Identification of proton transfer pathways in the X-ray crystal structure of the bacterial reaction center from *Rhodobacter sphaeroides*. Photosynth. Res. *55*, 119–125.

Ädelroth, P., Paddock, M.L., Sagle, L.B., Feher, G., and Okamura, M.Y. (2000). Identification of the proton pathway in bacterial reaction centers: both protons associated with reduction of Q_B to Q_BH_2 share a common entry point. Proc. Natl. Acad. Sci. USA *97*, 13086–13091.

Ädelroth, P., Paddock, M.L., Tehrani, A., Beatty, J.T., Feher, G., and Okamura, M.Y. (2001). Identification of the proton pathway in bacterial reaction centers: decrease of proton transfer rate by mutation of surface histidines at H126 and H128 and chemical rescue by imidazole identifies the initial proton donors. Biochemistry *40*, 14538–14546.

Alexov, E.G., and Gunner, M.R. (1999). Calculated protein and proton motions coupled to electron transfer: electron transfer from Q_A^- to Q_B in bacterial photosynthetic reaction centers. Biochemistry *38*, 8253–8270.

Alexov, E., Miksovska, J., Baciou, L., Schiffer, M., Hanson, D.K., Sebban, P., and Gunner, M.R. (2000). Modeling the effects of mutations on the free energy of the first electron transfer from Q_A^- to Q_B in photosynthetic reaction centers. Biochemistry *39*, 5940–5952.

Allen, J.P. (1994). Crystallization of the reaction center from *Rhodobacter sphaeroides* in a new tetragonal form. Proteins *20*, 283–286.

Antosiewicz, J., McCammon, J.A., and Gilson, M.K. (1996). The determinants of pK_as in proteins. Biochemistry *35*, 7819–7833.

Axelrod, H.L., Abresch, E.C., Paddock, M.L., Okamura, M.Y., and Feher, G. (2000). Determination of the binding sites of the proton transfer inhibitors Cd^{2+} and Zn^{2+} in bacterial reaction centers. Proc. Natl. Acad. Sci. USA *97*, 1542–1547.

Baciou, L., and Michel, H. (1995). Interruption of the water chain in the reaction center from *Rhodobacter sphaeroides* reduces the rates of the proton uptake and of the second electron transfer to Q_B. Biochemistry *34*, 7967–7972.

Beroza, P., Fredkin, D.R., Okamura, M.Y., and Feher, G. (1992). Proton transfer pathways in the reaction center of *Rhodobacter sphaeroides*: a computational study. In The Photosynthetic Bacterial Reaction Center II, J. Breton and A. Vermeglio, eds. (New York: Plenum Press), pp. 363–374.

Beroza, P., Fredkin, D.R., Okamura, M.Y., and Feher, G. (1995). Electrostatic calculations of amino acid titration and electron transfer, $Q_A^-Q_B \rightarrow Q_AQ_B^-$, in the reaction center. Biophys. J. *68*, 2233–2250.

Blankenship, R.E., Madigan, M.T., and Bauer, C.E. (1995). Anoxygenic photosynthetic bacteria, Volume 2 (Dordrecht, The Netherlands: Kluwer Academic Publishers).

Brunger, A.T., Adams, P.D., Clore, G.M., DeLano, W.L., Gros, P., Grosse-Kunstleve, R.W., Jiang, J.-S., Kuszewski, J., Nilges, N., Pannu, N.S., et al. (1998). Crystallography & NMR system (CNS): a new software system for macromolecular structure determination. Acta Crystallogr. D *54*, 905–921.

Buchanan, S.K., Fritzsch, G., Ermler, U., and Michel, H. (1993). New crystal form of the photosynthetic reaction centre from *Rhodobacter sphaeroides* of improved diffraction quality. J. Mol. Biol. *230*, 1311–1314.

Calvo, R., Abresch, E.C., Bittl, R., Feher, G., Hofbauer, W., Isaacson, R.A., Lubitz, W., Okamura, M.Y., and Paddock, M.L. (2000). EPR study of the molecular and electronic structure of the semiquinone biradical $Q_A^-{\cdot}Q_B^-{\cdot}$ in photosynthetic reaction centers from *Rhodobacter sphaeroides*. J. Am. Chem. Soc. *122*, 7327–7341.

CCP4 (Collaborative Computational Project 4) (1994). The CCP4 suite: programs for protein crystallography. Acta Crystallogr. D *50*, 760–763.

Decoursey, T.E. (2003). Voltage-gated proton channels and other proton transfer pathways. Physiol. Rev. *83*, 475–579.

Ermler, U., Fritzsch, G., Buchanan, S.K., and Michel, H. (1994). Structure of the photosynthetic reaction centre from *Rhodobacter sphaeroides* at 2.65 Å resolution: cofactors and protein-cofactor interactions. Structure *2*, 925–936.

Esnouf, R.M. (1999). Further additions to MolScript version 1.4, including reading and contouring of electron-density maps. Acta Crystallogr. D. *55*, 938–940.

Feher, G., Allen, J.P., Okamura, M.Y., and Rees, D.C. (1989). Structure and function of bacterial photosynthetic reaction centers. Nature *339*, 111–116.

Fritzsch, G., Koepke, J., Diem, R., Kuglstatter, A., and Baciou, L. (2002). Charge separation induces conformational changes in the photosynthetic reaction centre of purple bacteria. Acta Crystallogr. D *58*, 1660–1663.

Gerencser, L., and Maroti, P. (2001). Retardation of proton transfer caused by binding of the transition metal ion to the bacterial reaction center is due to pK_a shifts of key protonatable residues. Biochemistry *40*, 1850–1860.

Graige, M.S., Paddock, M.L., Bruce, J.M., Feher, G., and Okamura, M.Y. (1996). Mechanism of proton-coupled electron transfer for quinone (Q_B) reduction in reaction centers of *Rb. sphaeroides*. J. Am. Chem. Soc. *118*, 9005–9016.

Gunner, M.R. (1991). The reaction center protein from purple bacteria-structure and function. Curr. Top. Bioenerg. *16*, 319–367.

Hanson, D.K., and Schiffer, M. (1998). Symmetry-related mutants in the quinone binding sites of the bacterial reaction center—the effects of changes in charge distribution. Photosynth. Res. *55*, 275–280.

Hanson, D.K., Baciou, L., Tiede, D.M., Nance, S.L., Schiffer, M., and Sebban, P. (1992). In bacterial reaction centers protons can diffuse to the secondary quinone by alternative pathways. Biochim. Biophys. Acta *1102*, 260–265.

Hanson, D.K., Tiede, D.M., Nance, S.L., Chang, C.H., and Schiffer, M. (1993). Site-specific and compensatory mutations imply unexpected pathways for proton delivery to the Q_B binding site of the photosynthetic reaction center. Proc. Natl. Acad. Sci. USA *90*, 8929–8933.

Hienerwadel, R., Grzybek, S., Fogel, C., Kreutz, W., Okamura, M.Y., Paddock, M.L., Breton, J., Nabedryk, E., and Mantele, W. (1995). Protonation of Glu L212 following Q_B^- formation in the photosyn-

thetic reaction center of *Rhodobacter sphaeroides*: evidence from time-resolved infrared spectroscopy. Biochemistry *34*, 2832–2843.

Hoff, A.J., and Deisenhofer, J. (1997). Photophysics of photosynthesis. Structure and spectroscopy of reaction centers of purple bacteria. Phys. Rep. *287*, 2–247.

Katona, G., Andreasson, U., Landau, E.M., Andreasson, L.E., and Neutze, R. (2003). Lipidic cubic phase crystal structure of the photosynthetic reaction centre from *Rhodobacter sphaeroides* at 2.35 Å resolution. J. Mol. Biol. *331*, 681–692.

Kleinfeld, D., Okamura, M.Y., and Feher, G. (1984). Electron transfer in reaction centers of *Rhodopseudomonas sphaeroides*. I. Determination of the charge recombination pathway of $D^+Q_AQ_B^-$ and free energy and kinetic relations between $Q_A^-Q_B$ and $Q_AQ_B^-$. Biochim. Biophys. Acta *766*, 126–140.

Labahn, A., Paddock, M.L., McPherson, P.H., Okamura, M.Y., and Feher, G. (1994). Direct charge recombination from $D^+Q_AQ_B^-$ to DQ_AQ_B in bacterial reaction centers from *Rhodobacter sphaeroides*. J. Phys. Chem. *98*, 3417–3423.

Lancaster, C.R. (2002). Wolinella succinogenes quinol: fumarate reductase-2.2 Å resolution crystal structure and the E-pathway hypothesis of coupled transmembrane proton and electron transfer. Biochim. Biophys. Acta *1565*, 215–231.

Lancaster, C.R., Michel, H., Honig, B., and Gunner, M.R. (1996). Calculated coupling of electron and proton transfer in the photosynthetic reaction center of *Rhodopseudomonas viridis*. Biophys. J. *70*, 2469–2492.

Lanyi, J.K., and Luecke, H. (2001). Bacteriorhodopsin. Curr. Opin. Struct. Biol. *11*, 415–419.

Leibl, W., Sinning, I., Ewald, G., Michel, H., and Breton, J. (1993). Evidence that serine L223 is involved in the proton transfer pathway to Q_B in the photosynthetic reaction center of *Rhodopseudomonas viridis*. Biochemistry *32*, 1958–1964.

Leslie, A.G.W. (1992). Recent Changes to the MOSFLM Package for Processing Film and Image Plate Data, Volume 26 (Warrington, UK: Daresbury Laboratory).

Luzzati, P.V. (1952). Traitement statistique des erreurs dans la determination des structures cristallines. Acta Crystallog. *5*, 802–810.

Maroti, P., Hanson, D.K., Baciou, L., Schiffer, M., and Sebban, P. (1994). Proton conduction within the reaction centers of *Rhodobacter capsulatus*: the electrostatic role of the protein. Proc. Natl. Acad. Sci. USA *91*, 5617–5621.

McAuley, K.E., Fyfe, P.K., Ridge, J.P., Isaacs, N.W., Cogdell, R.J., and Jones, M.R. (1999). Structural details of an interaction between cardiolipin and an integral membrane protein. Proc. Natl. Acad. Sci. USA *96*, 14706–14711.

McRee, D.E. (1999). XtalView/Xfit: a versatile program for manipulating atomic coordinates and electron density. J. Struct. Biol. *125*, 156–165.

Merritt, E.A., and Bacon, J.D. (1997). Raster3D photorealistic molecular graphics. Methods Enzymol. *277*, 505–524.

Miksovska, J., Valerio-Lepiniec, M., Schiffer, M., Hanson, D.K., and Sebban, P. (1998). In bacterial reaction centers, a key residue suppresses mutational blockage of two different proton transfer steps. Biochemistry *37*, 2077–2083.

Mills, D.A., and Ferguson-Miller, S. (2003). Understanding the mechanism of proton movement linked to oxygen reduction in cytochrome c oxidase: lessons from other proteins. FEBS Lett. *545*, 47–51.

Nabedryk, E., Breton, J., Joshi, H.M., and Hanson, D.K. (2000). Fourier transform infrared evidence of proton uptake by glutamate L212 upon reduction of the secondary quinone Q_B in the photosynthetic reaction center from *Rhodobacter capsulatus*. Biochemistry *39*, 14654–14663.

Neutze, R., Pebay-Peyroula, E., Edman, K., Royant, A., Navarro, J., and Landau, E.M. (2002). Bacteriorhodopsin: a high-resolution structural view of vectorial proton transport. Biochim. Biophys. Acta *1565*, 144–167.

Okamura, M.Y., and Feher, G. (1995). Proton-coupled electron transfer reactions of Q_B in RCs. In Anoxygenic Photosynthetic Bacteria, R.E. Blankenship, M.T. Madigan, and C.E. Bauer, eds. (Dordrecht, The Netherlands: Kluwer), pp. 577–594.

Okamura, M.Y., Paddock, M.L., Graige, M.S., and Feher, G. (2000). Proton and electron transfer in bacterial reaction centers. Biochim. Biophys. Acta *1458*, 148–163.

Paddock, M.L., Rongey, S.H., Abresch, E.C., Feher, G., and Okamura, M.Y. (1988). Reaction centers from three herbicide resistant mutants of *Rhodobacter sphaeroides* 2.4.1: sequence analysis and preliminary characterization. Photosynth. Res. *17*, 75–96.

Paddock, M.L., Rongey, S.H., Feher, G., and Okamura, M.Y. (1989). Pathway of proton transfer in bacterial reaction centers: replacement of glutamic acid 212 in the L subunit by glutamine inhibits quinone (secondary acceptor) turnover. Proc. Natl. Acad. Sci. USA *86*, 6602–6606.

Paddock, M.L., McPherson, P.H., Feher, G., and Okamura, M.Y. (1990). Pathway of proton transfer in bacterial reaction centers: replacement of serine-L223 by alanine inhibits electron and proton transfers associated with reduction of quinone to dihydroquinone. Proc. Natl. Acad. Sci. USA *87*, 6803–6807.

Paddock, M.L., Rongey, S.H., McPherson, P.H., Juth, A., Feher, G., and Okamura, M.Y. (1994). Pathway of proton transfer in bacterial reaction centers: role of aspartate-L213 in proton transfers associated with reduction of quinone to dihydroquinone. Biochemistry *33*, 734–745.

Paddock, M.L., Senft, M.E., Graige, M.S., Rongey, S.H., Turanchik, T., Feher, G., and Okamura, M.Y. (1998). Characterization of second site mutations show that fast proton transfer to Q_B^- is restored in bacterial reaction centers of *Rhodobacter sphaeroides* containing the Asp-L213→Asn Lesion. Photosynth. Res. *55*, 281–291.

Paddock, M.L., Graige, M.S., Feher, G., and Okamura, M.Y. (1999). Identification of the proton pathway in bacterial reaction centers: inhibition of proton transfer by binding of Zn^{2+} or Cd^{2+}. Proc. Natl. Acad. Sci. USA *96*, 6183–6188.

Paddock, M.L., Feher, G., and Okamura, M.Y. (2000). Identification of the proton pathway in bacterial reaction centers: replacement of Asp-M17 and Asp-L210 with Asn reduces the proton transfer rate in the presence of Cd^{2+}. Proc. Natl. Acad. Sci. USA *97*, 1548–1553.

Paddock, M.L., Ädelroth, P., Chang, C., Abresch, E.C., Feher, G., and Okamura, M.Y. (2001). Identification of the proton pathway in bacterial reaction centers: cooperation between Asp-M17 and Asp-L210 facilitates proton transfer to the secondary quinone (Q_B). Biochemistry *40*, 6893–6902.

Paddock, M.L., Sagle, L., Tehrani, A., Beatty, J.T., Feher, G., and Okamura, M.Y. (2003). Mechanism of proton transfer inhibition by Cd^{2+} binding to bacterial reaction centers: determination of the pK_a of functionally important histidine residues. Biochemistry *42*, 9626–9632.

Pokkuluri, P.R., Laible, P.D., Deng, Y.L., Wong, T.N., Hanson, D.K., and Schiffer, M. (2002). The structure of a mutant photosynthetic reaction center shows unexpected changes in main chain orientations and quinone position. Biochemistry *41*, 5998–6007.

Rabenstein, B., Ullmann, G.M., and Knapp, E.W. (1998). Energetics of electron-transfer and protonation reactions of the quinones in the photosynthetic reaction center of *Rhodopseudomonas viridis*. Biochemistry *37*, 2488–2495.

Rongey, S.H., Paddock, M.L., Feher, G., and Okamura, M.Y. (1993). Pathway of proton transfer in bacterial reaction centers: second-site mutation Asn-M44→Asp restores electron and proton transfer in reaction centers from the photosynthetically deficient Asp-L213→Asn mutant of *Rhodobacter sphaeroides*. Proc. Natl. Acad. Sci. USA *90*, 1325–1329.

Sebban, P., Maroti, P., Schiffer, M., and Hanson, D.K. (1995). Electrostatic dominoes: long distance propagation of mutational effects in photosynthetic reaction centers of *Rhodobacter capsulatus*. Biochemistry *34*, 8390–8397.

Sham, Y.Y., Muegge, I., and Warshel, A. (1999). Simulating proton translocations in proteins: Probing proton transfer pathways in the *Rhodobacter sphaeroides* reaction center. Proteins *36*, 484–500.

Silverman, D.N. (2000). Marcus rate theory applied to enzymatic proton transfer. Biochim. Biophys. Acta *1458*, 88–103.

Stowell, M.H., McPhillips, T.M., Rees, D.C., Soltis, S.M., Abresch, E., and Feher, G. (1997). Light-induced structural changes in photosynthetic reaction center: implications for mechanism of electron-proton transfer. Science *276*, 812–816.

Takahashi, E., and Wraight, C.A. (1990). A crucial role for Asp^{L213} in the proton transfer pathway to the secondary quinone of reaction centers from *Rhodobacter sphaeroides*. Biochim. Biophys. Acta *1020*, 107–111.

Takahashi, E., and Wraight, C.A. (1992). Proton and electron transfer in the acceptor quinone complex of *Rhodobacter sphaeroides* reaction centers: characterization of site-directed mutants of the two ionizable residues, GluL212 and AspL213, in the Q_B binding site. Biochemistry *31*, 855–866.

Takahashi, E., and Wraight, C.A. (1996). Potentiation of proton transfer function by electrostatic interactions in photosynthetic reaction centers from *Rhodobacter sphaeroides*: First results from site-directed mutation of the H subunit. Proc. Natl. Acad. Sci. USA *93*, 2640–2645.

Utschig, L.M., Ohigashi, Y., Thurnauer, M.C., and Tiede, D.M. (1998). A new metal-binding site in photosynthetic bacterial reaction centers that modulates Q_A to Q_B electron transfer. Biochemistry *37*, 8278–8281.

Accession Numbers

The RCSB Protein Data Bank accession number for: (1) the *DN(L213)* mutant RC refined to 2.10 Å in the trigonal form is 1RY5, (2) the dark-adapted *DN(L213)/RC(M233)* revertant RC refined to 1.80 Å in the trigonal form is 1RZH, (3) the dark-adapted *DN(L213)/RC(M233)* revertant RC refined to 2.40 Å in the tetragonal form is 1RZZ, (4) the light-adapted *DN(L213)/RC(M233)* revertant RC refined to 2.60 Å in the tetragonal form is 1S00, and (5) the dark-adapted *DN(L213)/RH(H177)* revertant RC refined to 2.75 Å in the trigonal form is 1RVJ.